Chapter

Effects of Medium Components on the Bulk Rheology and on the Formation of Ferning Patterns for Biofilm of *Pseudomonas aeruginosa*

Uranbileg Daalkhaijav, Angela L. Dunham and Travis W. Walker

Abstract

Pseudomonas aeruginosa virulence and success within a broad range of hosts are largely due to the strength of its biofilms. The rheology of biofilm of *P. aeruginosa* was measured to investigate the bacterial response to nutritional conditions (medium that was modified with glycerol, glucose, sucrose, sodium chloride, and silver nitrate). The elastic modulus and the yield stress of the biofilm of *P. aeruginosa* increased in response to increases in glycerol, glucose, and sodium chloride. Alternatively, silver nitrate and glycerol inhibited biofilm formation at concentrations that were greater than 0.1 mM and 10 v/v%, respectively. Ferning patterns form as a result of diffusion-limited desiccation of the salt-macromolecule solution. Ferning coverage of about 50% and an orthogonal ferning pattern with 3° of branching were found for most of the biofilm samples. The complexity increased with modifications that caused strengthening of the biofilm, while the coverage and complexity dropped to zero when no biofilm growth was observed. The birefringent bundles of liquid crystals in the biofilm gained a new level of complexity and order within the ferning pattern that correlates with the biofilm robustness as characterized by its rheology, and these properties are heavily influenced by the nutritional environment of *P. aeruginosa*.

Keywords: biofilms, biorheology, ferning, birefringence

1. Introduction

A vast majority of microorganisms in the world exist within biofilms, which are weak hydrogels that often form at various interfaces [1]. The biofilms consist of up to 98% water, and they are typically composed of polymicrobial aggregates that are encased in extrapolymeric substances (EPS) [2–5]. Besides acting as a protective barrier, the EPS, which is made of DNA, proteins, and polysaccharides, aid in adhesion and water retention [4]. *Pseudomonas aeruginosa* is a well-known opportunistic human pathogen that is a common cause of hospital-acquired infections in burn wounds and eyes [6–8], and it is known to create persistent infection in cystic fibrosis (CF) patients [8–15], having resistance to many classes of antibiotics

[16–18]. PAO1, a medically-relevant strain of *P. aeruginosa* that is used in this study, acts as the model for biofilm-forming bacteria. To grow, bacterial cultures need water, a source of carbon, a source of nitrogen, and trace amounts of salts. The lysogeny broth (LB) is a complex and non-selective medium; many different types of bacteria can grow on non-selective medium. Lysogeny broth was formulated by Giusseppe Bertani in 1951 to optimize *Shigella* growth, but it has since become the standard for growing many bacterial cultures [19]. Lysogeny broth is composed of: 1% tryptone (source of amino acids); 0.5% yeast extract (source of vitamins, amino acids, nitrogen, and carbon); [20] and 1% NaCl (provides osmotic balance) [21]. Yeast extract is made from baker's yeast (*Saccharomyces cerevisiae*) grown to a high concentration and then exposed to high temperature or osmotic shock, killing the yeast and starting autolysis of the cells through the yeast's own enzymes [20, 22, 23]. The resulting extract solution is further filtered and spray-dried into a powder [20]. Proteins make up the most significant component of the powdered yeast extract at 62.5–73.8 wt% [20]. The average molecular weight of the yeast extract is 438 Da with 59.1% of the total under 300 Da [23]. Using additions of glycerol, glucose, sucrose, sodium chloride (NaCl), and silver nitrate ($AgNO_3$), this paper investigates various modifications of the LB medium for their effects on the biofilm.

Both the biofilm's structure and the cell-to-cell communication mechanism of the bacteria, known as quorum sensing (QS), are affected by their environment and the medium composition [24]. Quorum sensing controls additional properties that influence biofilm structures of bacteria, such as the production of extracellular DNA, proteins, mucus, and lipids [24–26]. When the growth environment becomes more viscous through the addition of glycerol, strains of *Pseudomonas* produced high-molecular-weight EPS and developed more robust biofilms [27]. The nutritional condition, such as the carbon source, influences the QS-associated swarming motility of *P. aeruginosa* [25]. While glucose supplementation limits bacterial motility, producing scattered, mushroom-like microcolonies, increasing the concentration of glucose from 0 to 2.7% caused an increase in the overall formation of biofilm [24, 25, 28, 29].

High osmolarity had a detrimental effect on biofilm of *P. fluorescens*, at roughly 0.4 Osm L^{-1} of either NaCl or sucrose, and the formation of biofilm decreased by four-fold as compared to lower concentrations of each component [30]. Similarly, mutant strains of *P. aeruginosa* that are found in CF patients transition from a non-mucoid to an alginate-overproducing state under osmotic stress that is induced by concentrations of 0.2–0.5 M NaCl (~1.2–3%) or 10% sucrose [31]. Silver has broad-spectrum antimicrobial effects on gram-negative bacteria that are well-documented [32, 33]. For instance, for concentrations of silver sulfadiazine that are lower than 0.16 μg mL^{-1}, planktonic growth of *P. aeruginosa* was unchanged; however, at or above this threshold amount, the concentration of the planktonic bacteria was reduced by five orders of magnitude [34]. Silver sulfadiazine was even effective against mature biofilms above a threshold dose of 1 μg mL^{-1}, and at concentrations of 10 μg mL^{-1}, it can completely eradicate a pre-established biofilm of *P. aeruginosa* [34].

The following sections of this study cover three different methods of characterizing biofilms: (i) rheology to quantify the impact of the modified medium on the mechanical strength of the biofilm; (ii) ferning to characterize the mass transport of the salts through the polymer matrix of the biofilm during desiccation; and (iii) birefringence to observe self-assembly behavior of the solute in the biofilm.

1.1 Rheology of biofilms

The study of flow and deformation of matter (rheology) enables characterization of its structure and mechanical properties. Rheology is an especially valuable

tool for understanding a vast range of "soft matter" that falls between liquid and solid phases [35]. Soft matter can be divided into four classes: (1) polymers, a long repeating chain of monomers which for biological samples include proteins, DNA, and cellulose; (2) colloids, a large category of materials that describe a suspension of one material into another medium such as aerosols, foams, emulsions, suspensions, and pastes; (3) amphiphiles, molecules with dual characteristics where one end of the molecule likes the solvent (hydrophilic), while the other end does not (hydrophobic) include surfactants that are amphiphiles at the air-water interface; and (4) liquid crystals, rod or disk shaped molecules that self-assemble to form orientation order but not positional order, resulting in an anisotropic fluid [35, 36].

Rheological techniques can characterize the strength and behavior of clinically relevant biological fluids such as mucus, blood plasma, and bacterial biofilm. More importantly, we can also use rheological measurements to drive the treatment of the biofluids toward a favorable clinical outcome. A rheological testing can quantify the viscous and elastic properties of a material. Two main modes of testing exist on a rotational rheometer: (1) steady-shear testing mode (**Figure 1a–d**), where the material is sheared between a stationary bottom plate and rotating top plate at a given stress or strain; and (2) the oscillation mode (**Figure 1e–g**), where the top plate oscillates back and forth at a set frequency and amplitude.

From the shear-flow sweep test, the stress (τ) versus shear rate ($\dot{\gamma}$) curve gives important information on the flow properties of the material (**Figure 1b**). The flow behavior can be modeled by Herschel-Bulkley function for yield stress fluids (Eq. (1): τ_y, yield stress; c [Pa s], flow coefficient or consistency index; p, power-law index). Yield stress materials have a minimum stress that must be surpassed before the material starts flowing. Different types of material flow behavior are described in **Figure 1b–d**.

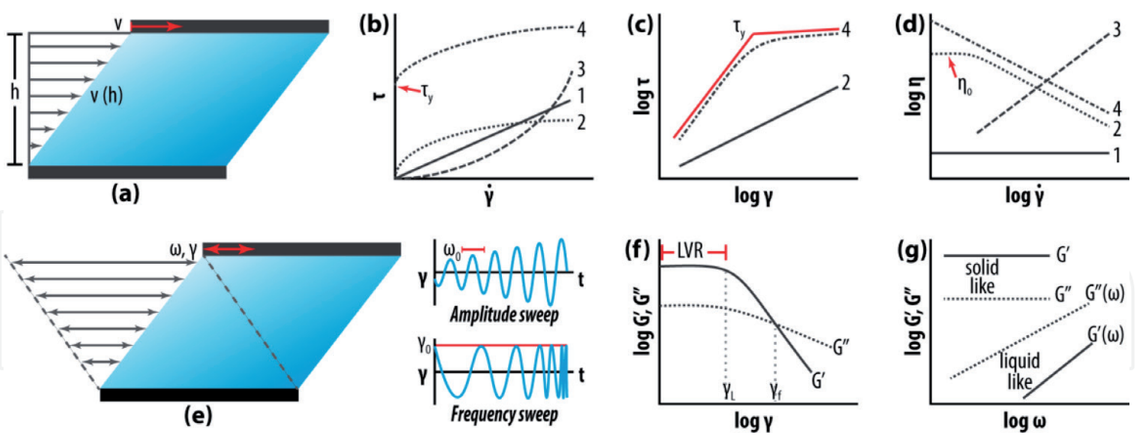

Figure 1.
Shear and oscillatory rheological techniques. (a) In a two-plate steady-shear system where the top plate is moving, the velocity (v) of the fluid is dependent on the gap height (h). (b) Samples can exhibit several different flow behaviors of stress versus strain rate, including (1) ideally viscous Newtonian fluid; (2) shear-thinning fluid; (3) shear-thickening fluid; and (4) yield stress fluid. Yield stress materials have a minimum stress (τ_y) that must be overcome before flow starts. (c) The stress-strain curve demonstrates a material with (2) no yield stress and (4) a material with a clear yield stress calculated using the tangent crossover point method. (d) The viscosity-shear rate plot shows (1) Newtonian fluid; (2) shear-thinning fluid with no yield stress reaching zero-shear viscosity (η_o); (3) shear-thickening fluid; and (4) shear-thinning fluid with yield stress. (e) In a two-plate system the top plate can oscillate back and forth at set amplitude or frequency for oscillatory rheology tests. The amplitude sweep test has constant frequency (ω_o) with changing strain amplitude while the frequency sweep test has constant strain amplitude (γ_o) with changing frequency. (f) During the amplitude sweep test, the strain values up to the limit of the strain where the G′ and G″ values are constant (γ_L) are called the linear viscoelastic region (LVR). The point where G″ crosses over G′ is called the flow point (γ_f) [72]. (g) In a frequency sweep, when G′ > G″ materials are said to be solid-like and when G″ > G′, materials are said to be liquid-like.

$$\tau = \tau_y + c * \dot{\gamma}^p \quad (1)$$

Two main types of oscillatory testing exist (**Figure 1e–g**). An amplitude sweep test oscillates the upper plate back and forth at a set frequency (ω_0) at increasing strains (**Figure 1e**). On the modulus (G′—elastic; G″—viscous) versus strain plot (**Figure 1f**), the plateau is the linear viscoelastic region (LVR), and the strain limit of the region is γ_L. A frequency sweep test oscillates at a set amplitude (γ_0), which has been determined previously from the amplitude sweep test to be within the LVR, at increasing frequency (**Figure 1e**). The frequency sweep describes how the material acts when the material is stressed for different periods. For example, when Silly Putty is stressed quickly by throwing it on the floor, it bounces back, acting like a rigid solid. However, when the Silly Putty sits at rest and experiences low stress over a long period of time, it spreads out, acting like a viscous fluid. The frequency sweep (**Figure 1g**) reveals if the material is solid-like (G′ > G″) or liquid-like (G″ > G′) and if the behavior is frequency dependent (G′(ω), G″(ω)) or independent. Stable gels and suspensions are typically solid-like and frequency-independent, so these types of materials are called "gel-like."

Previous studies on biofilm rheology using various techniques of rheological measurement have found the elastic modulus (G′) to range in order of magnitude from 10^{-2} to 10^4 Pa for bulk biofilms at solid-liquid interfaces using plate-on-plate methods, while the values of yield stress (τ_y) range in order of magnitude from 10^{-1} to 10^5 Pa [2, 37–42]. The wide-ranging values of G′ and τ_y in the literature reflect the variability in the compositions of the biofilms, diversity of growth mediums, variability of growth conditions, and most importantly, natural variability of response of the microorganisms, even to the same medium and growth conditions. This chapter uses the techniques established in our previously published work on the non-destructive development and characterization of rheological properties of biofilms [43]. Using this non-destructive method, the measured values of elastic modulus and yield stress of PAO1 that were grown in standard LB medium were both between 0.1 and 10 Pa [43].

1.2 Crystallization of biological materials

Biological fluids like tears, cervical mucus, and saliva are all shown to self-assemble into fractal-like patterns of crystallization when they are dried [44, 45]. A fractal is a structure that is made of smaller parts that resemble the bigger parts, with a high degree of organization and self-similarity. This structure can be characterized with a specific fractal dimension [44]. Fractal dimension is a measure of complexity of the fractal pattern [46]. Random nucleations of salts initiate the process of crystallization, where its growth is limited by the diffusion of salt through the polymer matrix (proteins or macromolecules) [47]. Therefore, the combined effects of ionic strength, osmolarity, and the size and concentration of macromolecules control the behavior of crystallization, where too little or too much of one factor can dramatically alter the pattern of crystallization [48, 49]. A typical crystallization of biosaline proceeds in the following manner: (i) salt nucleation initiates the process of crystallization; (ii) the nucleation point grows with some symmetry into a highly-branched structure whose growth is modified by the interaction of the salt with the biological matter; (iii) the branches do not overlap or merge [47, 50, 51]. The process of crystallization of biofluids is called "arborization," "ferning," or "dendritic growth" in various literature [45]. In this paper, the general formation of salt crystals will continue to be called crystallization, while the specific crystallization of the biofluids that result in fractal patterns will be called ferns.

The ferning patterns of the dried samples of tears and saliva have been used for years as a supplementary diagnostic tool [49, 52]. The ferning patterns in saliva and in tears exhibit different morphologies; saliva produces linear ferns with branching angles of 90°, while ferns from tears have more curvature with tightly packed branches with acute angles. Ferning patterns from tears and saliva are traditionally classified in a qualitative manner according to Rolando's system as Type I to Type IV [53]. Type I has the most ferning and the highest concentration of protein, while Type IV has no ferning and the lowest amount of protein [49]. Samples of tears from healthy individuals typically exhibit robust, highly-branched ferning patterns (Type I and II), while samples from patients with eye or immune diseases show little to no ferning (Type III and IV) [48, 49, 52]. Through analysis of X-ray microscopy and scanning electron microscopy (SEM), the molecular structure of the ferns from tears is revealed to be composed of NaCl, KCl, and proteins [48]. In addition to helping detect infection, saliva ferning pattern has been shown to be useful for tracking ovulation cycle from highest fertility level during estrus to lowest fertility level during diestrus [54].

Cervical mucus is a heterogeneous hydrogel that changes over the course of an animal's reproductive cycle [44, 45, 55]. Regardless of the source, human or otherwise, high levels of estrogen are produced during ovulation or peak fertility, resulting in linear ferns with branching angles of 90°, while no ferning is found during the period of low fertility when progesterone is dominant [44, 45]. During ovulation, the cervical mucus is over 98% water with its highest level of salt while both water content and salt content drops during low fertility period [45]. The low salt content during low fertility period is the cause of the lack of ferning pattern.

SEM analysis of ferns from gelatin-NaCl mixture revealed that the backbone of the ferning pattern was a series of interlocking crystalline blocks that were 10–30 μm in size [47]. When the fractal dimension of bovine cervical mucus (BCM) that was taken during ovulation was determined using the box-counting method, it was about 1.7, characteristic of diffusion-limited growth processes [44, 46]. Box counting method is based on counting non-empty boxes making up a fractal pattern on a grid [46]. A diffusion limitation was observed with the gelatin-NaCl mix as well. The ferning pattern became much less geometric and increasingly random at higher gelatin-to-NaCl ratios, where more diffusion limitation occurs due to the crosslinking of the gelatin, and the ferning ceased at extremely high gelatin-to-NaCl ratios [47]. Furthermore, the ferning pattern developed curvatures at evaporation rates above a threshold value of 11 μm s^{-1} [47].

Bacterial biofilms produce ferning patterns that are similar to gelatin and mucus samples [50, 56]. Upon evaporation of droplets of solutions of various salts with cells of *E. coli* and *Bacillus subtilis*, ferning patterns emerged where the crystallized top layer covered a base layer that consisted of bacterial cells. The structure of the *E. coli* ferns was linear with branching angles of 90°, similar to cervical mucus. Neither sterile saline solutions nor *E. coli* in pure water produced ferning, confirming the previous findings that ferning results from balanced proportions of salts and macromolecules [50, 56]. Bacteria inside the crystalline structure were effectively in a state of suspended animation that was capable of reanimation after rehydration, even a week later [50]. This crystallization was hypothesized to be a form of biomineralization [50], which occurs when biological organisms produce organo-mineral hybrids that give the organism mechanical strength and hardness. Examples of biomineralization that are found in nature include bones, teeth, shells, corals, and algal silica [57]. Previous studies on strain PAO1 of *P. aeruginosa* in flow cell reactors have shown biomineralization of calcium carbonate within the EPS of the biofilm [58]. SEM of the ferning sample of *E. coli* revealed a 3D structure that was composed of dried EPS, bacteria, and salts, with the salts concentrated in the crystalline region, consistent with the previously mentioned studies [50].

Studying the ferning pattern and complexity of biofluids or biogels gives a simple and indirect measurement of the structures within the material that guide or hinder the movement of ions that ultimately form these distinct crystallization patterns. While much of the ferning patterns seen in biofluids are linear patterns with 90° branching angles, tightly packed and curved ferning patterns can be expected to develop in environments that induce fast evaporation such as in low-viscosity fluids or environments that are highly diffusion limited such as in high macromolecule to salt ratio fluids.

1.3 Birefringence of *P. aeruginosa*

One of the techniques of self-assembly for small particles is through depletion attraction in a solvent during solvent evaporation [59, 60]. Depletion attraction is an entropic force that becomes relevant when the particles in the solvent move close enough together that their excluded volumes overlap [61]. This overlap increases the osmotic pressure in the surrounding fluid and further pushes the particles together [59]. These highly ordered or anisotropic solution is described as having a liquid crystal phase and this phase is birefringent, which means that their ordered state will split light into two beams with perpendicular polarization [36, 60, 62]. Liquid crystal phases have been observed with many different types of biopolymers such as DNA, peptides, glycopolymers, proteoglycans, viruses, collagen, cellulose, phages, and chitin [60, 61, 63]. Liquid crystals form: (i) nematic phase where the molecules form directional order but no positional order; (ii) smectic phase with positional order; or (iii) chiral phase with twisting order [60]. Of these, biopolymers most commonly have nematic phase.

P. aeruginosa that exists in a viscous or anaerobic environment is stimulated to transcribe filamentous Pf bacteriophages that are about 2 μm in length and 6 nm in diameter [64]. In *P. aeruginosa* biofilm, the filamentous phage self-assembles through depletion attraction, with the biopolymers exerting the osmotic force that bundles the phage strands. These highly ordered anisotropic regions of nematic phase liquid crystals are birefringent, possessing a large negative charge, and the anisotropy was shown to increase with the ionic strength and the molecular weight [64, 65]. Birefringence is not only a direct indicator of molecular order, but it is an indicator for *P. aeruginosa* biofilm strength, surface adhesivity, desiccation tolerance, and antibiotic resistance [62, 64]. The filamentous bacteriophages facilitate chronic infection of *P. aeruginosa* in the host by promoting a less invasive, less inflammatory but more resistant, more persistent form of *P. aeruginosa* [66]. In addition, Pf phages can bind iron to inhibit the metabolic activity of other pathogens such as *Aspergillus fumigatus* [67].

Liquid crystal methods provide the means to study the structure and behavior of filamentous bacteriophages without perturbation [65]. Moreover, liquid crystal analysis, specifically through detection of its birefringence, was used to detect analytes such as glucose, cholesterol, *E. coli*, and even viruses such as Ebola and HIV [68]. This detection method was made possible through enzymatic reaction in response to analytes within the mesophase of the normally optically isotropic lipidic cubic phases that results in the formation of strongly birefringent liquid crystal phases that are easily detected optically [68]. The exogenous and endogenous birefringence from various classes of analytes were exploited to make simple and cheap detection tool that was proposed as a new diagnostic tool that can be utilized in industry or in the field to detect biothreats [68].

1.4 Objective

Biofilm is composed of motile bacterial cells, non-motile bacterial aggregates, and mucoid hydrogels of EPS that have a heterogeneous, highly-porous microstructure,

allowing diffusion of water, nutrients, waste, and electrolytes [26, 69]. A complex set of interactions between the electrolytes, solutes, bacteria, and biopolymers dictate the strength, bacterial resistance, and infection persistence of the biofilm. The objective of this study is to characterize the behavior of the bacterial culture in the presence of various environmental conditions, including a highly viscous media, nutrient-enhanced media, high osmolarity media, and antimicrobial media. The interaction of the bacterial culture with its nutrient environment is measured as a function of the strength of its biofilm through rheological analysis, while its ferning pattern characterizes the mass transport through the environment in the biofilm. Additionally, birefringence inside a biofilm provides insight into the solute interaction with the biofilm.

2. Materials and methods

2.1 Bacterial strains, media, and growth conditions

The strain of *Pseudomonas aeruginosa* that was used for the entire study was the laboratory-adapted wild-type strain, PAO1. Miller lysogeny broth (LB) was prepared from BD Difco dry powder and autoclaved. Five different types of chemical modifications were made to the lysogeny broth: (i) glycerol was added to form between 1 and 15 v/v% in LB medium; (ii) glucose was added to form concentrations between 0.5 and 4.5 w/v% in LB; (iii) sucrose was added to form concentrations between 0.5 and 4.5 w/v% in LB; (iv) NaCl added to form concentrations between 1.5 and 5 w/v% in LB; and (v) $AgNO_3$ added to form concentrations between 0.001 and 1 mM in LB. Modified LB medium in a petri dish (3.6 mL) was inoculated with an overnight culture of PAO1 (0.4 mL) and was incubated for 6 days at 37°C. Some of the dishes of modified LB medium were kept sterile and incubated along with the biofilm samples to act as a negative control.

2.2 Measuring bulk biofilm rheology

The sample rheology was measured on the Discovery Hybrid Rheometer 3 (DHR3, TA Instruments, USA) using a 40-mm stainless steel plate geometry at 25°C. The measurements took place in the following order:

a. Pre-stressed: 0.1 Pa, 2 minutes

b. Frequency sweep: $\gamma_0 = 0.1$ (biofilm), $\gamma_0 = 0.005$ (sterile LB), $\omega \in [0.01, 1]$ rad s^{-1}

c. Stress sweep: $\tau \in [0.01, 1]$ Pa (biofilm), $\tau \in [0.001, 0.1]$ Pa (sterile LB), terminating if the shear rate $\dot{\gamma} > 10\ s^{-1}$.

Detailed description of the sample inoculation, the incubation, and the rheological measurement methods are located in our previous work [43].

2.3 Ferning properties of dried bacterial biofilms

The biofilm samples were dried in the incubator, forming ferning patterns that were large enough to be easily seen by the unaided eye. In this paper, the previous qualitative method for ferning characterization was converted to a quantitative method of image analysis by calculating the coverage area, the fractal dimension, and the complexity score (degree of branching) of the ferning pattern. This analysis was completed by taking photographs of the surface of the petri dish, converting

the photographs to black and white image on MATLAB (Figure S4, https://ir.library.oregonstate.edu/concern/defaults/g158bp85b), and finally calculating the ferning coverage by determining the ratio between white and black pixel areas in the image. The fractal dimension was calculated using the box-counting method on MATLAB (Figure S4, https://ir.library.oregonstate.edu/concern/defaults/g158bp85b).

2.4 Dried bacterial biofilms under the microscope

Microscopic images of the biofilm in its liquid and its dried ferning state were taken using an Eclipse Ti-S inverted microscope (Nikon, Japan). The polarized images were produced with polarized filters.

3. Results and analysis

3.1 Rheological characterization of biofilms

3.1.1 Sweeps of frequency

Data from the sweeps of frequency showed the difference in the viscoelasticity of the samples of biofilm (filled square) and the samples of sterile LB medium (unfilled circle) that were incubated for 6 days (**Figure 2**). For brevity, the term "unmodified LB" will refer to the standard LB medium without chemical alterations, while "modified LB" will refer to any of the five chemical additions to standard LB medium (glycerol, glucose, sucrose, NaCl, and $AgNO_3$). The sweep of frequency of the biofilm showed frequency-independent, elastic modulus (G') dominance over the viscous modulus (G'') for all of the samples, as expected for a weak gel (Figure S3, https://ir.library.oregonstate.edu/concern/defaults/g158bp85b). The complex modulus $\left(|G^*| = |\sqrt{G'^2 + G''^2}|\right)$ for the samples of biofilm (~0.02 Pa) were, on average, an order of magnitude larger than their counterparts of sterile LB medium (**Figure 2a**). Previous work on the sterile LB medium showed that aging and cycling of temperature can cause buildup of protein at the air-liquid interface, which can be measured by a plate geometry to an extent, though not as accurately as using a du Noüy ring. Therefore, the measurable viscoelasticity in the sterile samples can be attributed to the age of the medium at the time of use (>3 months) and to the incubation process, which further accelerated the aging. The complex modulus of the unmodified LB biofilm and the sterile unmodified LB medium were each averaged over the entire frequency range (0.1–1 rad s^{-1}) and were averaged between replicates (biofilm n = 12, sterile n = 7) to get mean values for G*. All the raw results from sweeps of frequency of the biofilm and of the sterile samples in modified LB medium (Figure S2, https://ir.library.oregonstate.edu/concern/defaults/g158bp85b) were averaged over the entire frequency range and plotted (Figure S3b–f, https://ir.library.oregonstate.edu/concern/defaults/g158bp85b). The mean values of G* for biofilms that were grown in unmodified LB (red) served as the base of comparison for biofilms that were grown in modified LB medium (**Figure 2b–f**). Based on the modulus data, bacterial biofilm appeared to be strongly affected by its nutritional environment.

3.1.2 Sweeps of stress

The values of yield stress were derived from the experiments of increasing strain, where the yield stress is the point of offset of a stress-versus-strain curve.

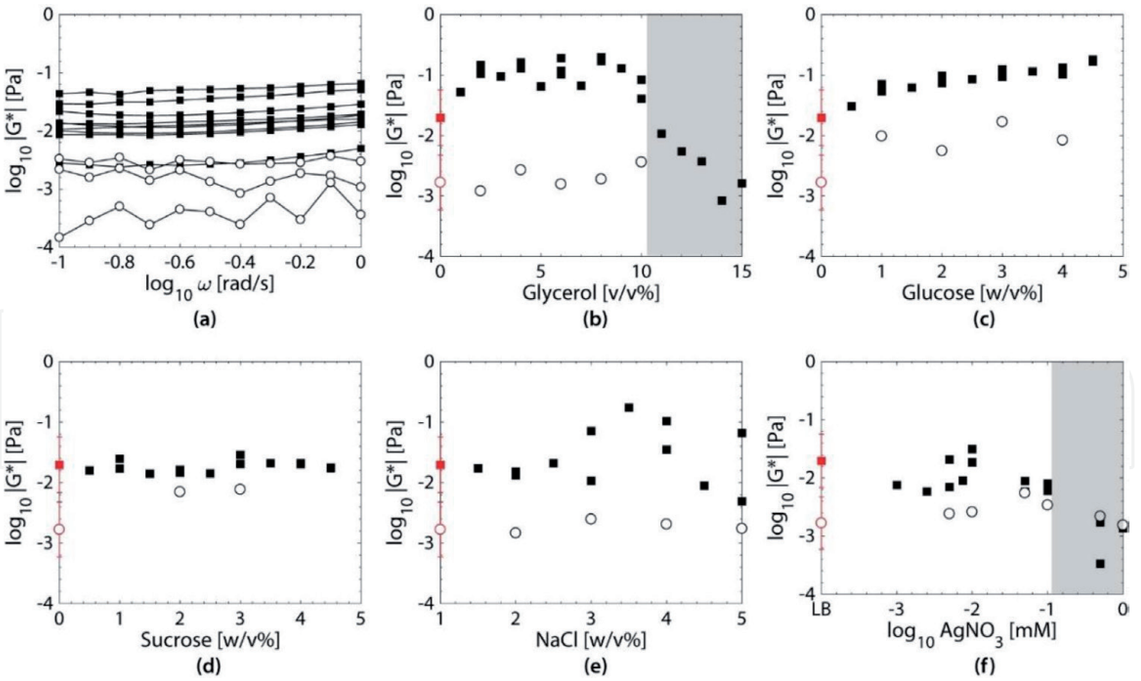

Figure 2.
Modulus |G| calculated from the sweep of frequency showing the biofilm (filled square) and sterile LB medium (unfilled circle) samples. The results of the (a) sweep of frequency from ω ∈[0.1, 1] rad s^{-1} (biofilm γ_o = 0.1 and sterile LB medium γ_o = 0.005) of biofilm samples that were grown in unmodified LB medium and of sterile unmodified LB medium. The mean modulus |G*| was 0.015 Pa for biofilm and 0.0015 Pa for sterile unmodified LB medium. (b–f) The mean modulus |G*| is plotted (red) with relative errors that were calculated from standard error to ensure symmetry (n ≥ 3). The average |G*| of biofilm that was grown in modified LB medium with the following concentrations (b) 1–15 v/v% glycerol, (c) 0.5–4.5 w/v% glucose, (d) 0.5–4.5 w/v% sucrose, (d) 1.5–5 w/v% NaCl and (e) 0.001–1 mM $AgNO_3$ are shown. The gray regions in (b) and (f) represent inhibiting concentrations that had no biofilm growth.*

The stress-versus-strain data of the unmodified LB biofilm (filled square) and sterile unmodified LB samples (unfilled circle) showed that the samples of biofilm exhibited an appreciable yield stress (**Figure 3a**). After yielding, the material stress was constant (<1 Pa) at high strain, while the samples of sterile medium demonstrated no yield stress. In fact, none of the sterile modified or unmodified LB mediums had an appreciable yield stress (Figure S2, https://ir.library.oregonstate.edu/concern/defaults/g158bp85b). The mean yield stress of the samples of unmodified LB biofilm (red) was compared with the biofilms that were grown on the modified LB medium (**Figure 3b–f**). The results of yield stress showed a similar dependence on the nutritional conditions of the biofilms as the results of the modulus from the sweeps of frequency.

3.1.3 Modification with glycerol

With the addition of glycerol (0–15 v/v%), the complex modulus of the biofilm increased by almost an order of magnitude between 0 and 2% glycerol, remained constant between 2 and 10%, and experienced a dramatic drop in modulus for concentrations greater than 10% to modulus values that are comparable to sterile LB (**Figure 2b**). The yield stress of the biofilm showed similar trends, increasing by one order of magnitude with glycerol from 0 to 10% until concentrations of glycerol that were greater than 10% impeded the growth of biofilm, also resulting in no yield stress (**Figure 3b**). The addition of glycerol increased the viscosity of the medium as well as inducing high osmolarity (1.4 Osm L^{-1} at 10%), promoting stronger biofilm. Other studies with glycerol-supplemented medium saw an increase in the production of EPS by biofilm, consistent with the present study [27, 70]. The glycerol can trigger

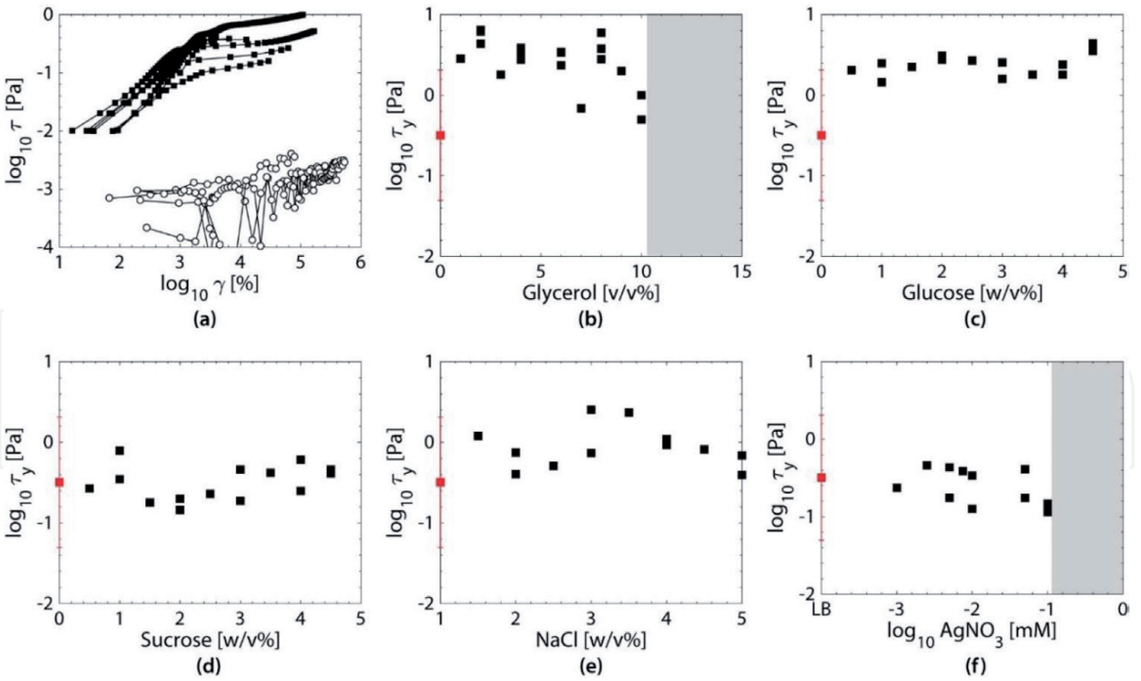

Figure 3.
(a) The stress versus strain data of biofilm that was grown in unmodified LB medium (filled square) and of samples of sterile unmodified LB medium (unfilled circle). (b–f) For the mean yield stress of biofilm that was grown in unmodified LB medium (red square), the standard error bars were converted to relative errors to ensure symmetry on the y-axis ($n \geq 7$). Plots of yield stress τ_y of the biofilms that were grown in modified LB medium at the following concentrations (b) 1–15 v/v% glycerol, (c) 0.5–4.5 w/v% glucose, (d) 0.5–4.5 w/v% sucrose, (e) 1.5–5 w/v% NaCl and (f) 0.001–1 mM $AgNO_3$ are shown. The mean τ_y was 0.32 Pa for the unmodified LB biofilms, while the LB medium did not have a yield stress. The gray regions in (b) and (f) represent inhibiting concentrations that had no biofilm growth.

pathways of production of EPS; [27] however, at high concentrations of glycerol, the diffusion-limiting environment of the highly viscous solution with high osmotic pressure (>4 Osm L^{-1} at >10%) appeared to inhibit growth. The complex modulus of the modified LB medium, on the other hand, stayed relatively constant with glycerol addition. The dramatic drop in the modulus of biofilm samples that were grown in medium that was modified with >10% glycerol corresponded with an apparent lack of biofilm in the Petri dishes, as the dishes appeared clear and yellow instead of opaque and greenish (Figure S1, https://ir.library.oregonstate.edu/concern/defaults/g158bp85b). The greenish hue in the samples is a result of the presence of pyocyanin, which is a bluish-tinted toxin that is produced by PAO1.

3.1.4 Modification with glucose

The modulus of the biofilm increased by one order of magnitude by increasing the concentration of glucose from 0 to 4.5% (**Figure 2c**), indicating that glucose was being utilized by the bacteria as an additional source of carbon which promoted growth and development of a stronger network of biofilm. The rheological results of the sterile glucose-modified LB medium did not change significantly from the unmodified LB medium. The values of yield stress followed the same trend, where the biofilm that was grown in glucose-modified LB medium had yield stresses that were an order of magnitude larger than the unmodified LB biofilm (**Figure 3c**). A previous study observed the same effect, finding that the addition of glucose up to the highest level tested, which was 2.7%, enhanced biofilm production [29]. The maximum addition of glucose (4.5%) induced osmotic pressure of 0.25 Osm L^{-1}, which did not cause inhibiting effects.

3.1.5 Modification with sucrose

Based on the rheology, sucrose did not increase biofilm production, as no change existed in the modulus (**Figure 2d**) or yield stress (**Figure 3d**) of the biofilm. In previous studies, concentrations of sucrose above 10% in medium for *P. aeruginosa* resulted in biofilm with mucoid development, while *P. fluorescens* started to experience adverse effects above 15% at which point the biofilm dramatically decreased [30, 31]. In those studies, bacterial culture reached an inhibiting level of sucrose at 15% due to osmotic pressure (0.44 Osm L^{-1}) [30]. In the present work, samples of PAO1 experienced a maximum of 0.13 Osm L^{-1} in osmotic pressure from modification with sucrose, which is well below the reported osmotic level for inhibition. *P. aeruginosa* may not be capable of utilizing sucrose, so in contrast to the simpler glucose, sucrose had little impact on the rheological properties of the biofilm.

3.1.6 Modification with sodium chloride

Unmodified LB medium already consists of sodium chloride (NaCl) at a concentration of 1%, and the modified concentration varied from 1 to 5% of NaCl. The complex modulus of biofilm remained constant for concentrations below 2.5% and increased by one order of magnitude for concentrations between 2.5 and 5%, while the modulus of the sterile modified LB medium was not affected by the concentration of NaCl (**Figure 2e**). Similarly, the yield stress increased as the concentration of NaCl was increased greater than 2.5% (**Figure 3e**). NaCl is already required for bacterial growth to provide osmotic balance, but a larger amount of salts appeared to promote stronger biofilm. The change in the biofilm could be caused by the higher salinity or osmolarity, making the environment hostile, triggering a higher level of production of alginate and other types of EPS as a countermeasure. Previous studies found that concentrations of NaCl between about 1 and 3% increased production of biofilms in *S. aureus* and *P. aeruginosa*, while concentrations of about 6% of NaCl prevented growth of biofilm in *S. aureus* [29, 31]. At concentrations of NaCl above 10%, no biofilm growth was observed, and the plate quickly crystalized to cubes of salt (Figure S6, https://ir.library.oregonstate.edu/concern/defaults/g158bp85b).

3.1.7 Modification with silver nitrate

Silver has antimicrobial properties that can inhibit bacterial growth and development of biofilm. Supplementation of silver nitrate ($AgNO_3$) to the modified LB medium has no impact on the complex modulus (**Figure 2f**) or the yield stress of the biofilm for concentrations below 0.1 mM (**Figure 3f**). Past this concentration, the modulus instantly reduced to the same level as the sterile modified LB medium, and the yield stress disappeared. Correspondingly, the plates of biofilm at the higher silver concentrations appeared clear and less viscous, resembling sterile modified LB medium (Figure S1, https://ir.library.oregonstate.edu/concern/defaults/g158bp85b). Therefore, the antimicrobial activity of the silver appeared to be strongly dependent on concentration, with little to no effect on bacterial growth at concentrations lower than the threshold (0.1 mM) and deadly at higher concentrations. These results are consistent with previous studies where the inhibitory threshold for *S. aureus* was over 0.033 mM, while the inhibitory threshold for *P. aeruginosa* was over 0.16 μg mL^{-1} (0.45 mM) [34, 71].

3.1.8 Summary of rheological characterization

The rheological parameters of elastic modulus and yield stress are useful measures of the strength of a biofilm. The complex modulus and the yield stress of the biofilms increased with the addition of glucose, which served as an additional source of carbon, but they were unaffected by addition of sucrose, which is a complex sugar that the bacteria could not utilize. The strength increased to an extent with osmolarity (glycerol and NaCl) and dramatically reduced to their sterile baseline at concentrations that were higher than the inhibitory threshold of an antimicrobial agent ($AgNO_3$). Samples with higher rheological properties correlated with a biofilm that appeared more viscous than the unmodified LB biofilm, while samples with lower modulus, and lacking a yield stress, such as high concentrations of glycerol and silver ions, appeared less viscous and free of biofilm. The values of modulus and yield stress for the samples of biofilm displayed the same medium dependent response; therefore, either measurement would be a useful metric of the strength of biofilm. Out of the five chemical modifications, three modifications increased the strength of the biofilm when compared to the unmodified LB biofilm: glycerol for concentrations up to 10%, glucose for concentrations at least up to 4.5%, and NaCl for concentrations higher than 2.5%. One of the chemicals, sucrose, had no measurable effect on the strength of the biofilm for concentrations at least up to 4.5%, while another modifier, $AgNO_3$, inhibited bacterial growth at a concentration above 0.1 mM.

3.2 Development of ferning patterns on dried plates of biofilm

After the plates were dried over a span of weeks in the incubator, they were photographed, and the photographs were converted to black and white images and cropped (Table S1, https://ir.library.oregonstate.edu/concern/defaults/g158bp85b). The patterns of crystallization on the plates were analyzed based on the ferning coverage of the plate and the complexity of the pattern (**Figure 4**). The complexity of the ferning was scored qualitatively by the degree of branching of the pattern (**Figure 4**): 0, empty plate, no ferning; 1, seed or nucleation points; 2, lines without branching; 3, orthogonal pattern with 1° of branching; 4, orthogonal pattern with 2° of branching; 5, orthogonal pattern with 3° of branching; 6, orthogonal pattern with 4° of branching; 7, orthogonal pattern with 5° of branching; and 8, dendritic pattern with branching at acute angles. The branches at acute angles were distinctly smaller, and they were irregularly branched when compared to the orthogonal ferns that were scored 3–7 on the complexity scale.

The ferning coverage was calculated quantitatively based on the percent of white pixels in the black and white images that were converted from its original photograph (**Figure 5a**). A photograph of the ferning on a plate of unmodified LB biofilm showed high ferning coverage (top photos), while the plate of sterile unmodified LB medium was noticeably absent of ferning with low calculated coverage (bottom photos). Even without biofilm growth, the sterile coverage values were not zero because the lighting and the glare of the plate surface produced some pixel artifacts. **Figure 5b–f** shows the mean coverage of the plates of unmodified LB biofilm (red filled square, n = 12) and of the plates of sterile unmodified LB medium (red unfilled circle, n = 7) plotted with the data of the modified LB medium. The left black y-axis is the ferning coverage, while the right gray y-axis is the qualitative ferning complexity score for biofilm (gray filled square) and the sterile LB medium (gray unfilled circle).

3.2.1 Modifications with glycerol

With the addition of glycerol, the ferning pattern of the samples of biofilm initially changed from a complexity score of 5 and a coverage of 47% (unmodified LB

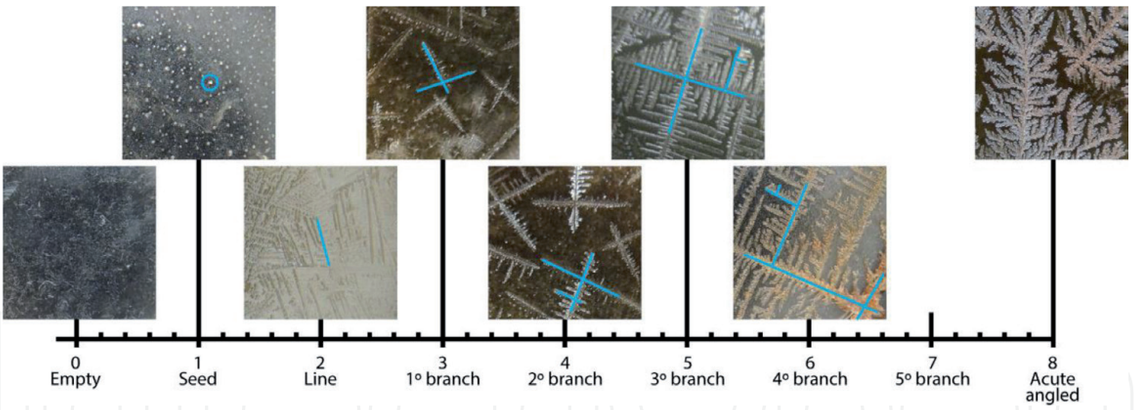

Figure 4.
A guide for the fernning complexity score of the dried biofilm fernning pattern.

biofilm) to a complexity score of 8 (**Figure 5b**). The change in fernning morphology from the orthogonal form to the acute branching form occurred at the lowest tested concentration of glycerol (**Figure 5b**: 2% plate, top left). However, as the concentration of glycerol increased, the fernning coverage dropped dramatically, reaching zero at around 8%. From both the visual inspection and the rheological measurement, samples below 10% had strong biofilm. However, a large amount of glycerol prevented the sample from completely drying, leaving the surface of the sample looking shiny and wet, causing both the fernning coverage and the complexity score to drop between 4 and 10% glycerol (**Figure 5b**: 10% plate, top right). The plates with concentrations of glycerol above 10% never dried, so no photographs were taken, and values of the coverage and complexity score were assumed to be zero. Sterile LB medium coverage and complexity score did not change from the unmodified values of about zero.

3.2.2 Modification with glucose

In samples that were modified with the addition of glucose, the fernning coverage remained consistent, while the complexity score changed from 5 to 8 at 2.5% and then held steady at higher concentrations of glucose (**Figure 5c**). The pattern on the plates transitioned from standard orthogonal fernning at low concentrations of glucose (**Figure 5c**: 0.5%, top left) to acute branching at high concentrations of glucose (**Figure 5c**: 4.5%, top right). The coverage and the complexity score on the sterile plate remained unchanged from the standard values.

3.2.3 Modification with sucrose

The desiccated plates of medium modified with sucrose had the most unusual patterns (**Figure 5d**). Both the coverage (47–30%) and the complexity score (5–3) dropped when the concentration of sucrose increased from 0 to 2%. However, with further increase from 2 to 4% sucrose, the coverage increased to 50%, while the complexity score continued to show less degrees of branching. Similar to glycerol, sucrose is hygroscopic, so plates appeared shinier and somewhat wet with increasing concentration of sucrose. At the same time, the fernning on the surface evolved (Table S1, https://ir.library.oregonstate.edu/concern/defaults/g158bp85b) from the orthogonal pattern (**Figure 5d**: 0.5%, top left) to fine strands to finally no fernning at high concentrations of sucrose (**Figure 5d**: 4.5%, top right). The glare in the photos from the shiny surface along with the packing of the fine crystalline strands produced high estimations of surface coverage until both the coverage and

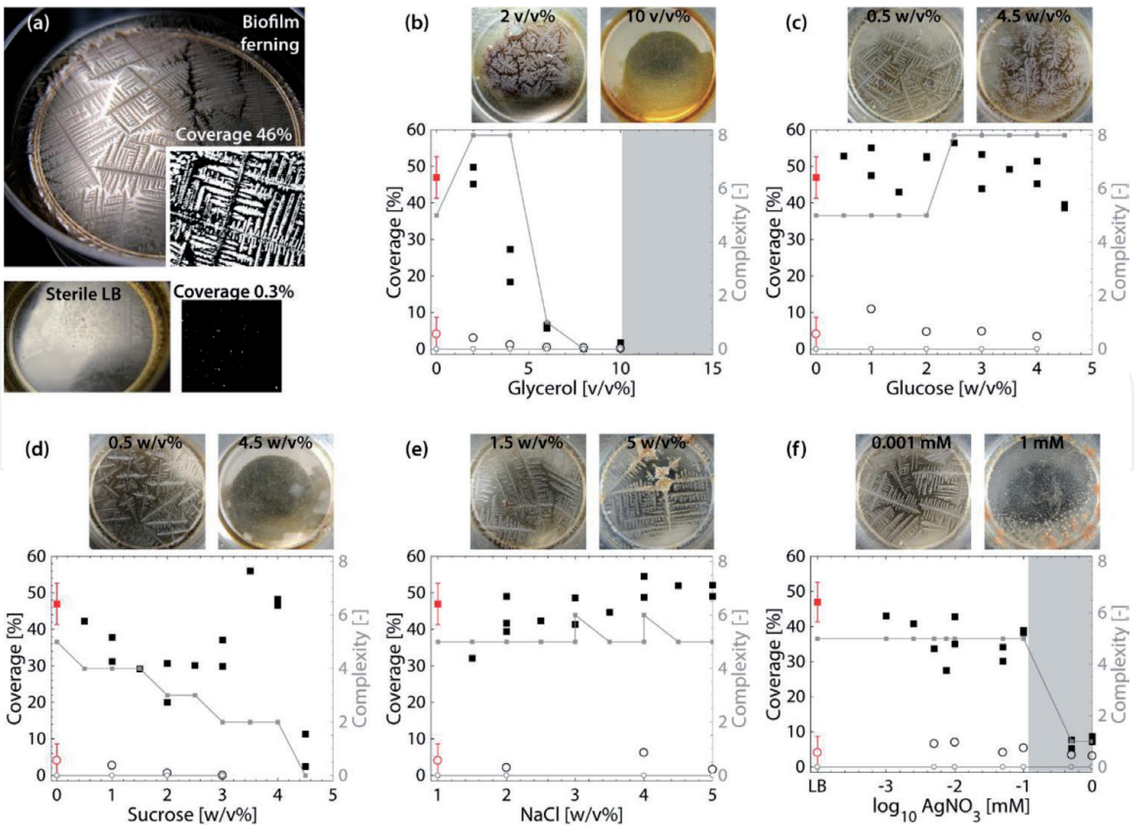

Figure 5.
(a) The original photograph was converted to a black and white image before the ferning coverage was calculated from the processed image. An example of ferns from biofilm that was grown in unmodified LB medium with 46.2% ferning coverage and from a plate of sterile unmodified LB medium showing zero ferning coverage. (b–f) Ferning coverage (left y-axis in black) and complexity score (right y-axis in gray) of biofilm that was grown in modified LB medium (coverage: black filled squares; complexity: Gray filled squares) and of sterile plates (coverage: black unfilled circles; complexity: Gray unfilled circles). The mean coverage and standard deviation of biofilm that was grown in unmodified LB medium (n = 12) and in sterile unmodified LB medium (n = 7) are plotted in red across figures (b–f). The results of the biofilm that was grown in modified LB medium with (b) glycerol, (c) glucose, (d) sucrose, (e) NaCl and (f) $AgNO_3$ are shown. The change in morphology of the biofilm ferning pattern with (b) glycerol at concentrations of 2% (top left) and 10% (top right); (c) glucose at concentrations of 0.5% (top left) and 4.5% (top right); (d) sucrose at concentrations of 0.5% (top left) and 4.5% (top right); (e) NaCl at concentrations of 1.5% (top left) and 5% (top right); and (f) $AgNO_3$ at concentrations of 0.001 mM (top left) and 1 mM (top right) are shown. The gray regions in (b) and (f) represent inhibiting concentrations that had no biofilm growth.

the complexity score suddenly dropped to zero at the maximum concentration of sucrose that was tested (4.5%). The complexity score of the pattern steadily dropped from 5 to 0 with sucrose, while the calculation of coverage resulted in scattered results, as the surface glare and the interaction of the densely packed linear striations with light affected the procedure.

3.2.4 Modification with sodium chloride

With further addition of sodium chloride (NaCl) to the modified LB medium, the ferning coverage remained consistently around 50%, and the complexity score remained around 5 (**Figure 5e**). Still, a change to the pattern exists, as the ferns evolved from thin branches (**Figure 5e**: 1.5%, top left) to a more pronounced branching with large crystalline formations with increasing concentration of NaCl (**Figure 5e**: 5%, top right). While the ferning branches became wider with the further addition of NaCl, the complexity score did not change. The orthogonal morphology and the non-overlapping crystallization appear to naturally limit the maximum coverage of the ferning pattern, resulting in a consistent 40–50% coverage. The sterile dishes with modified LB medium that contained the same amount

of salt did not produce fernning patterns, so the coverage and complexity score remained zero.

3.2.5 Modification with silver nitrate

The complexity score for the plates that were treated with silver nitrate ($AgNO_3$) remained 5 for concentrations below 0.1 mM, but at higher concentrations, no biofilm growth occurred, resulting in a complexity score of 1 (**Figure 5f**). Even with no measurable biofilm, the plates contained clusters of dried materials that resembled nucleation points (**Figure 5f**: 1 mM, top right). For concentration below 0.1 mM of silver nitrate, the fernning patterns were orthogonal (**Figure 5f**: 0.001 mM, top left), and the coverage was in the range of 30–40%. Finally, the coverage dropped below 10% at concentrations that were greater than the inhibiting concentration of 0.1 mM. The coverage did not completely drop to 0, as beige clusters were left behind on the plate, which was the same reason that the complexity score was 1 for the highest concentration even though no biofilm was present.

3.2.6 Summary of fernning patterns

Similar to the dependence of rheological properties of the biofilm on the nutrient environment, the fernning pattern was dependent on the properties of the bacterial biofilm, so it changed with the composition of the medium. No fernning existed on plates that lacked biofilm. The presence of biofilm, confirmed rheologically and visually, correlated with robust fernning patterns. Using the same box-counting method, fernning patterns on the samples of unmodified LB biofilm had a fractal dimension of 1.8 (Figure S5, https://ir.library.oregonstate.edu/concern/defaults/g158bp85b), which is consistent with samples of mucus that had a fractal dimension of 1.7 [44]. The plates of sterile medium that were incubated and dried under the same conditions as the plates of biofilm had no visible fernning pattern, no yield stress, and little to no elastic modulus. So, the medium composition not only affected the growth of the biofilm and its rheological properties but also, by extension, affected the fernning pattern.

The complexity score and the fernning coverage was higher for stronger biofilms (higher G^* and τ_y) that caused more limitations in mass transfer, and both values dropped to nearly zero when no biofilm was present. The morphology of ferns with a complexity score of 8 that were produced by the biofilms with higher elasticity was similar to random/acute-angled branching ferns that were produced under conditions of increased diffusion limitation in a previous study [47]. Exceptions were the plates that appeared to never fully dry due to the high concentration of hygroscopic materials like sucrose or glycerol. So, even as the rheological properties of the biofilm increased (glycerol) or stayed constant (sucrose), the complexity score and coverage dropped with increasing amounts of the modifying chemical. The fernning coverage never exceeded 60%, indicating a natural growth limitation that was based on the available space and the morphology of the ferns. The videos of the fernning process demonstrated how these branches quickly started and stopped growing without any of the branches overlapping (Video S1, https://ir.library.oregonstate.edu/concern/defaults/g158bp85b).

The fernning patterns of the biofilms were large (visible without microscopy on the order of centimeters) with most of the patterns consisting of orthogonal branches, and the ferns were reproducible in coverage and complexity score. The fernning patterns that were formed by the biofilm had the same morphology as fernning patterns of saliva, cervical mucus, *E. coli*, salt-gel, or salt-protein [44, 47, 49, 50]. From reports in the literature and the results in this work, the orthogonal

or oblique branching seemed to be the most common type of ferning with the examples of branches with acute angles being rare [47]. The cause of the change in the morphology of the fern in biofilms from 90° angles to acute angles is not immediately clear. However, other studies have reported that the gelatin-to-salt ratio was the key factor controlling the ferning morphology of salt-gelatin mixtures [47]. Therefore, the samples with higher rheological properties (glycerol and glucose samples), which arguably has a higher amount of EPS, may have produced branching with acute angles due to the increased EPS-to-salt ratio. Thus, the acute-angle morphology dominated when the biofilms had larger rheological values, indicating higher EPS-to-salt ratio, while orthogonal-branching morphology dominated at intermediate ratios with no ferning at extremely high or low values of the EPS-to-salt ratio.

3.3 Birefringence of bacterial biofilms

Analyzing the pre-desiccation biofilm that was grown in 5% NaCl under polarized filters showed the entire sample sample lit with birefringent strands (**Figure 6**). The Pf bacteriophages produced by *P. aeruginosa* are known to self-assemble into liquid crystals that exhibit birefringence [64]. The birefringent strands (black arrows) are 50–100 μm in length, and they are evenly distributed throughout the sample (**Figure 6a** and **b**). A magnified view of the strands revealed that each strand was a bundle of smaller strands that were surrounded by cell clusters (yellow arrows) and biofilm (**Figure 6c**). The bacteriophages are about 6 μm in length, so the bundle was likely composed of hundreds of individual Pf phages that were assembled into one strand [64]. These birefringent strand clusters did not exist in samples lacking biofilm. A plate with 10% NaCl LB medium formed sheets of salt crystals, no visible biofilm, and no birefringent strands (Figure S6, https://ir.library.oregonstate.edu/concern/defaults/g158bp85b).

The 5% NaCl sample that was previously analyzed (**Figure 6**) was desiccated (**Figure 7a**) and examined with and without a polarized filter (**Figure 7b–k**). The red lines outlined the specific regions of the fern under the microscope. The region outlined in the circle (**Figure 7b–e**) was the square crystalline structure on the plate. Without a filter this region showed a cubic structure with a length of 4–5 mm per side with a nucleation point in the center and thin diagonal lines running through it with cavernous voids coming from the sides of the structure (**Figure 7b**). The center of the ferning structure showed cuboid lattice-like patterns of growth emerging from the seed point (**Figure 7e**). Similarly, the previous study of the ferning pattern in a gelatin-salt mix revealed interlocking salt blocks with a length of 10–30 μm on a side that formed the backbone of the ferning structure [47].

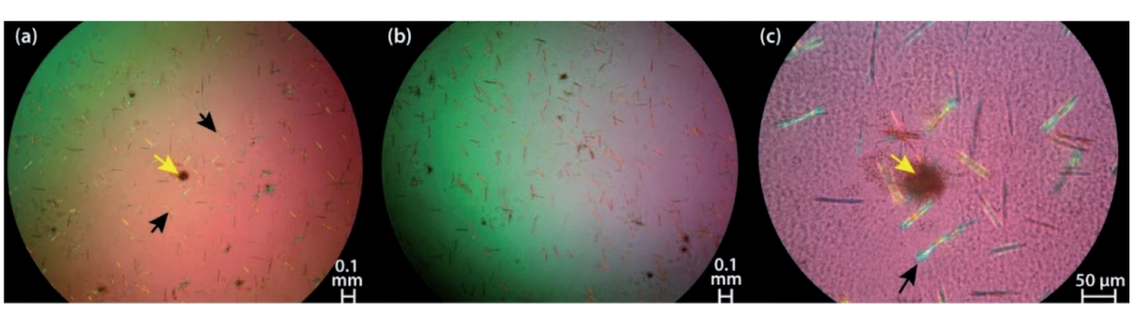

Figure 6.
Polarized microscopic images of inoculated samples of PAO1 in modified LB medium with a concentration of 5% NaCl. (a and b) Birefringent fragments exist throughout the liquid medium. (c) The birefringent thread-like fragments (black arrows) of about 50–100 μm in length were dispersed within medium that was full of bacterial clusters (yellow arrows).

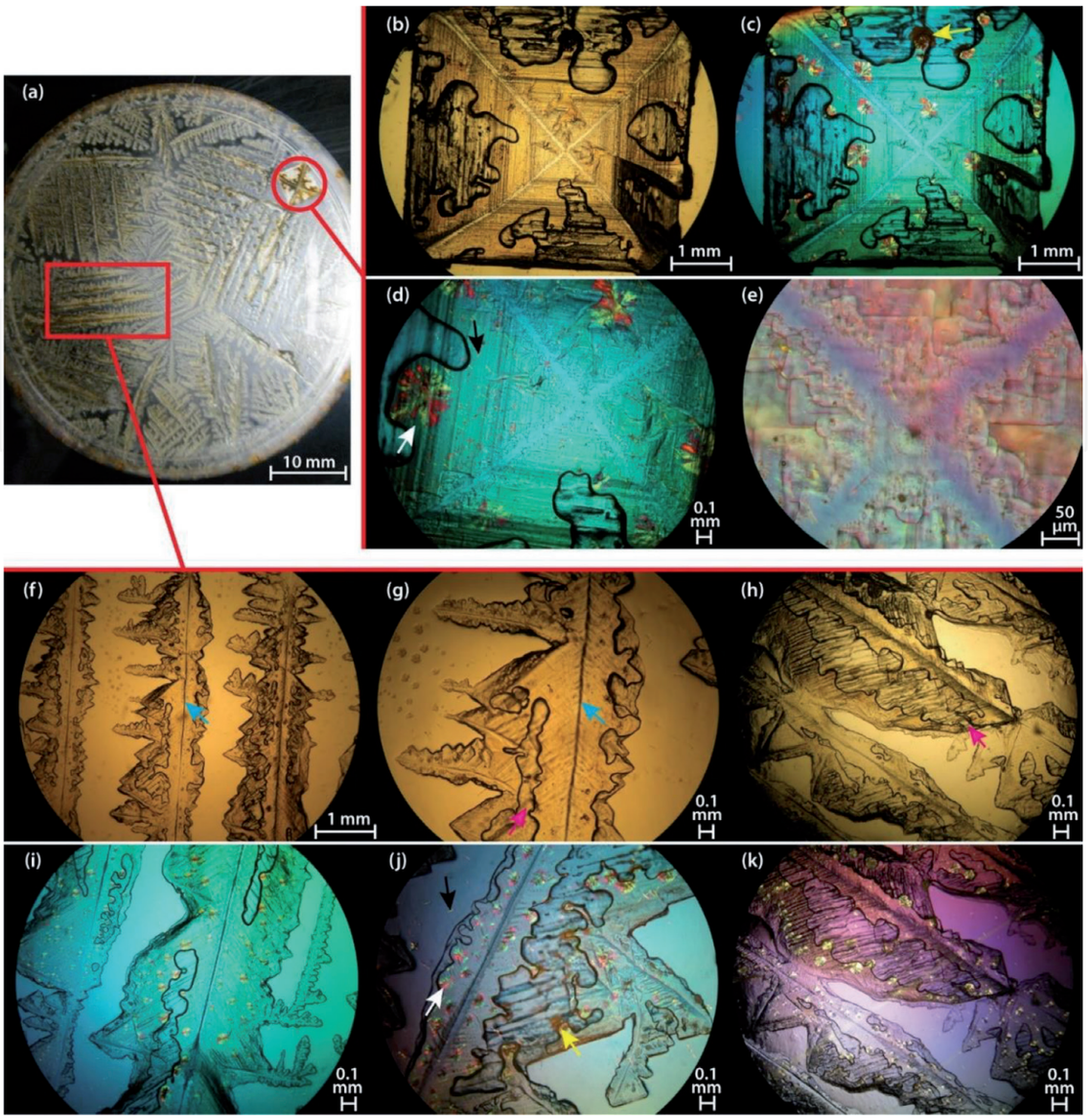

Figure 7.
Desiccated biofilm that was grown in LB medium with 5% NaCl. (a) Fernig pattern from the bottom of the petri dish. The regions that are outlined in red were inspected under the microscope. (b–e) The cubic piece at the top right corner of the plate (red circle): (b) seen under normal light; (c and d) seen through a polarized filter at different magnifications; (e) focused on the seed point of crystallization. (f and k) The fernig region of the plate (red square): (f–h) different regions of the fern under normal light at different magnifications; (i and j) seen through a polarized filter at different magnifications; (k) viewed at a different angle of polarization.

With a polarized filter, bright birefringent regions lit throughout the square (**Figure 7c**). A closer look at the center of the square revealed two forms of birefringent structures, large red and gold star formations (~0.5 mm in diameter) and red and gold strands that were about 50 µm in diameter (**Figure 7d**). In contrast to the birefringent strands that were scattered throughout the sample (black arrows), the birefringent stars (white arrows) were only in the crystallized ferns. Each birefringent strand that was visible in **Figure 7c** was a bundle of even smaller birefringent strands (**Figure 6c**). Therefore, the formation of the birefringent star demonstrated that having an even higher order of self-assembly during desiccation was possible such that the bundled strands further merged into a star formation. The alternating red and gold coloring indicated that the strands with matching orientations cluster together, but they must not have formed the entire cluster, as no star formation existed with only one color.

From the linear ferning section that was outlined by the red square (**Figure 7f–k**), the branches appeared to be about 1 mm in width with a distinct centerline running through each branch (**Figure 7f**). A magnified view of one of these branches revealed latticed or layered networks emanating from this central line (blue arrows) and cavities (pink arrows) that were present throughout the structure (**Figure 7g**). Some of the cavities were large, tunneling deep into the ferning structure (**Figure 7h**). Under polarized light, the branch was shown to have dozens of the star-shaped red and gold birefringent bundles (**Figure 7i**). Changing the angle of the polarized filter changed the color of the birefringent region from red and gold to gold and green (**Figure 7k**). The star-shaped birefringent clusters only existed within the crystal regions of the fern pattern, while the strands were scattered throughout the plate regardless of the ferning pattern (**Figure 7j**). This localization of the morphologies implied that the birefringent strands were produced within the biofilm; thus, they could be found throughout the material, while the formations of the birefringent stars were created as a result of crystallization, so they were only found within the crystalline regions. Clusters of bacterial cells appeared to be entrapped within the crystallized fern (yellow arrows), especially around the extremities of the ferning structure (**Figure 7c** and **j**). Similarly entrapped bacterial clusters were capable of reanimation at least a week after desiccation within the ferning structure [50]. Therefore, clusters of *P. aeruginosa* that were seen in **Figure 7c** and **j** may be in a suspended animation state as well, though this hypothesis was not tested during this study.

4. Conclusions

In environments that contained high viscosity (glycerol), high osmolarity (glycerol, NaCl), and high concentrations of simple carbon (glucose), the elasticity and the yield stress of the biofilm increased. Silver nitrate had an inhibiting effect on the biofilm formation, but only at concentrations that were greater than 0.1 mM. Similarly, concentrations of glycerol greater than 10% completely inhibited biofilm growth. However, the complex carbon structure of sucrose meant that it could not be utilized as an additional carbon source by PAO1 in the same way that glucose was utilized. Therefore, sucrose did not change the rheological properties of the biofilm. So, *P. aeruginosa* developed stronger biofilm under nutrient-rich conditions, certain levels of osmotic stress, and certain levels of diffusion limitation. However, it would not develop biofilm when the osmotic stress or diffusion limitation exceeded an inhibition amount or when an antimicrobial agent exceeded its inhibition concentration.

While the rheological properties of biofilm revealed information about the strength of the biofilm, the morphology of the ferning pattern best described the interactions between the electrolytes and the EPS in the biofilm. Typically, the biofilm had ferning coverage of about 50% and a ferning complexity score of 5. The ferning complexity increased with the strength of the biofilm (high complex modulus and yield stress), as stronger biofilm increased diffusion limitation that was experienced by the solutes within the matrix. The coverage and complexity score both dropped to zero when no biofilm formed, so the macromolecule-to-salt ratio was too low for ferning to occur, as with high concentrations of silver nitrate and glycerol. Many of the analysis methods of biofluid ferning patterns were qualitative and subjective, which is currently problematic considering its use as an indicator of certain medical symptoms. The image analysis and ferning classification method that was presented here could easily be applied to the other fields to give more quantitative values to the analysis of ferning biofluids.

The birefringence that was produced by liquid crystals within the samples of biofilm had two different morphologies, bundled strands that were about 50 μm in length in hydrated biofilm and star-shaped bundle of strands that were almost ten times larger inside the crystalline region of the fernning pattern. So, in addition to the self-assembly of the phages to strands inside the biofilm, a more complex assembly took place during crystallization in the biofilm that produced this tertiary structure. During the fernning process, clusters of bacteria became entrapped within the crystalline phase. Other researchers have found that these entrapped bacteria are in suspended animation state and that they could be brought back to life upon rehydration. If PAO1 can also reanimate, then fernning is yet another mechanism that *P. aeruginosa* could utilize to survive extreme conditions, similar to how liquid crystals formed by phages enhanced the resistance and persistence of *P. aeruginosa*.

Acknowledgements

The authors would like to thank Dr. Skip Rochefort for consulting on the rheology tests and Kristin Marshall for her help with the image conversion work. Additionally, the authors would like to thank Marisa Thierheimer, Curran Gahan, and Dalton Myas for helping with experimental preparation.

Conflict of interest

We do not have any conflict of interests to declare.

Funding

This work would not be possible without funding from Medical Research Foundation of Oregon.

Supplemental materials

The supplemental documents for this section may be found at: https://ir.library.oregonstate.edu/concern/defaults/g158bp85b.

Author details

Uranbileg Daalkhaijav[1], Angela L. Dunham[1] and Travis W. Walker[2*]

1 School of Chemical, Biological, and Environmental Engineering, Oregon State University, Corvallis, Oregon, USA

2 Department of Chemical and Biological Engineering, South Dakota School of Mines and Technology, Rapid City, South Dakota, USA

*Address all correspondence to: travis.walker@sdsmt.edu

IntechOpen

References

[1] Vu B, Chen M, Crawford RJ, Ivanova EP. Bacterial extracellular polysaccharides involved in biofilm formation. Molecules. 2009;**14**(7):2535-2554

[2] Lieleg O, Caldara M, Baumgärtel R, Ribbeck K. Mechanical robustness of *Pseudomonas aeruginosa* biofilms. Soft Matter. 2011;**7**(7):3307-3314

[3] Hall-Stoodley L, Costerton JW, Stoodley P. Bacterial biofilms: From the natural environment to infectious diseases. Nature Reviews Microbiology. 2004;**2**(2):95-108

[4] Flemming H-C, Wingender J. The biofilm matrix. Nature Reviews Microbiology. 2010;**8**(9):623-633

[5] Wloka M, Rehage H, Flemming H-C, Wingender J. Rheological properties of viscoelastic biofilm extracellular polymeric substances and comparison to the behavior of calcium alginate gels. Colloid & Polymer Science. 2004;**282**(10):1067-1076

[6] Yuan SJ, Pehkonen SO. Microbiologically influenced corrosion of 304 stainless steel by aerobic *Pseudomonas* NCIMB 2021 bacteria: AFM and XPS study. Colloids and Surfaces B: Biointerfaces. 2007;**59**:87-99

[7] Schuster M, Greenberg EP. A network of networks: Quorum-sensing gene regulation in *Pseudomonas aeruginosa*. International Journal of Medical Microbiology. 2006;**296**(2-3):73-81

[8] Silby MW, Winstanley C, Godfrey SAC, Levy SB, Jackson RW. Pseudomonas genomes: diverse and adaptable. FEMS Microbiology Reviews. 2011;**35**(4):652-680

[9] Barraud N, Hassett DJ, Hwang S-H, S a R, Kjelleberg S, Webb JS. Involvement of nitric oxide in biofilm dispersal of *Pseudomonas aeruginosa*. Journal of Bacteriology. 2006;**188**(21):7344-7353

[10] Palmer KL, Aye LM, Whiteley M. Nutritional cues control *Pseudomonas aeruginosa* multicellular behavior in cystic fibrosis sputum. Journal of Bacteriology. 2007;**189**(22):8079-8087

[11] Mowat E, Paterson S, Fothergill JL, Wright EA, Ledson MJ, Walshaw MJ, et al. *Pseudomonas aeruginosa* population diversity and turnover in cystic fibrosis chronic infections. American Journal of Respiratory and Critical Care Medicine. 2011;**183**(12):1674-1679

[12] Lau GW, Hassett DJ, Ran H, Kong F. The role of pyocyanin in *Pseudomonas aeruginosa* infection. Trends in Molecular Medicine. 2004;**10**(12):599-606

[13] Rada B, Leto TL. Pyocyanin effects on respiratory epithelium: Relevance in *Pseudomonas aeruginosa* airway infections. Trends in Microbiology. 2013;**21**(2):73-81

[14] Ghafoor A, Hay ID, Rehm BHA. Role of exopolysaccharides in *Pseudomonas aeruginosa* biofilm formation and architecture. Applied and Environmental Microbiology. 2011;**77**(15):5238-5246

[15] Folkesson A, Jelsbak L, Yang L, Johansen HK, Ciofu O, Høiby N, et al. Adaptation of *Pseudomonas aeruginosa* to the cystic fibrosis airway: An evolutionary perspective. Nature Reviews Microbiology. 2012;**10**(12):841-851

[16] Livermore DM. Multiple mechanisms of antimicrobial resistance in *Pseudomonas aeruginosa*: Our worst nightmare? Clinical Infectious Diseases. 2002;**34**(5):634-640

[17] Davies D. Understanding biofilm resistance to antibacterial agents.

Nature Reviews Drug Discovery. 2003;**2**(2):114-122

[18] Berk V, Fong JCN, Dempsey GT, Develioglu ON, Zhuang X, Liphardt J, et al. Molecular architecture and assembly principles of vibrio cholerae biofilms. Science. 2012;**337**(6091):236-239

[19] Bertani G. Lysogeny at mid-twentieth century: P1, P2, and other experimental systems. Journal of Bacteriology. 2004;**186**(3):595-600

[20] Acumedia. Yeast Extract (7184); 2011

[21] Bertani G. Studies on lysogenesis. I. The mode of phage liberation by lysogenic Escherichia coli. Journal of Bacteriology. 1951;**62**:293-300

[22] BD Biosciences. BD Bionutrients™ Technical Manual—Advanced Bioprocessing; 2006

[23] Organo Technie. Standard Series: Yeast Extract 19512; 2008

[24] De Kievit TR. Quorum sensing in *Pseudomonas aeruginosa* biofilms. Environmental Microbiology. 2009;**11**(2):279-288

[25] Shrout JD, Chopp DL, Just CL, Hentzer M, Givskov M, Parsek MR. The impact of quorum sensing and swarming motility on *Pseudomonas aeruginosa* biofilm formation is nutritionally conditional. Molecular Microbiology. 2006;**62**(5):1264-1277

[26] Schuster M, Sexton DJ, Diggle SP, Greenberg EP. Acyl-homoserine lactone quorum sensing: From evolution to application. Annual Review of Microbiology. 2013;**67**:43-63

[27] Shemesh M, Chaia Y. A combination of glycerol and manganese promotes biofilm formation in Bacillus subtilis via histidine kinase KinD signaling. Journal of Bacteriology. 2013;**195**(12):2747-2754

[28] Klausen M, Aaes-Jørgensen A, Molin S, Tolker-Nielsen T. Involvement of bacterial migration in the development of complex multicellular structures in *Pseudomonas aeruginosa* biofilms. Molecular Microbiology. 2003;**50**(1):61-68

[29] Lim Y, Jana M, Luong TT, Lee CY. Control of glucose-and NaCl-induced biofilm formation by rbf in Staphylococcus aureus. Journal of Bacteriology. 2004;**186**(3):722-729

[30] O'Toole GA, Kolter R. Initiation of biofilm formation in Pseudomonas fluorescens WCS365 proceeds via multiple, convergent signalling pathways: A genetic analysis. Molecular Microbiology. 1998;**28**(3):449-461

[31] Damkiær S, Yang L, Molin S, Jelsbak L. Evolutionary remodeling of global regulatory networks during long-term bacterial adaptation to human hosts. Proceedings of the National Academy of Sciences of the United States of America. 2013;**110**(19):7766-7771

[32] Ferreira C, Pereira AM, Melo LF, Simões M. Advances in industrial biofilm control with micro-nanotechnology. Current Research, Technology and Education Topics in Applied Microbiology and Microbial Biotechnology. 2010;**2**:845-854

[33] Raulio M. Ultrastructure of Biofilms Formed by Bacteria from Industrial Processes. Helsinki: University of Helsinki; 2010

[34] Bjarnsholt T, Kirketerp-Møller K, Kristiansen S, Phipps R, Nielsen AK, Jensen PØ, et al. Silver against *Pseudomonas aeruginosa* biofilms. APMIS. 2007;**115**(8):921-928

[35] Larson RG. The Structure and Rheology of Complex Fluids. New York, Oxford: Oxford University Press; 1999. 688 p

[36] Hamley IW. Introduction to Soft Matter (Revised Ed.). Introduction to Soft Matter: Synthetic and Biological Self-Assembling Materials. Chichester, UK: John Wiley & Sons, Ltd; 2007. pp. 1-328

[37] Pavlovsky L, Younger JG, Solomon MJ. In situ rheology of Staphylococcus epidermidis bacterial biofilms. Soft Matter. 2013;**9**(1):122

[38] Towler BW, Rupp CJ, Cunningham AB, Stoodley P. Viscoelastic properties of a mixed culture biofilm from rheometer creep analysis. Biofouling. 2003;**19**(5):279-285

[39] Vinogradov AM, Winston M, Rupp CJ, Stoodley P. Rheology of biofilms formed from the dental plaque pathogen Streptococcus mutans. Biofilms. 2004;**1**(1):49-56

[40] Kovach K, Davis-Fields M, Irie Y, Jain K, Doorwar S, Vuong K, et al. Evolutionary adaptations of biofilms infecting cystic fibrosis lungs promote mechanical toughness by adjusting polysaccharide production. npj Biofilms and Microbiomes. 2017;**3**(1):1

[41] Shaw T, Winston M, Rupp CJ, Klapper I, Stoodley P. Commonality of elastic relaxation times in biofilms. Physical Review Letters. 2004;**93**(9):098102

[42] Houari A, Picard J, Habarou H, Galas L, Vaudry H, Heim V, et al. Rheology of biofilms formed at the surface of NF membranes in a drinking water production unit. Biofouling. 2008;**24**(4):235-240

[43] Daalkhaijav U, Walker TW. Developing a nondestructive technique for measuring bulk rheology of p*seudomonas Aeruginosa* biofilm. Applied Rheology. 2017;**27**(6):64033-64043

[44] Cortés ME, Hauyón R, González F, Vigil P. Evidence of fractality in a pattern of crystallization of bovine cervical mucus obtained at oestrus. International Journal of Morphology. 2012;**30**(4):1461-1465

[45] Cortés ME, González F, Vigil P. Crystallization of bovine cervical mucus at oestrus: An update. Revista de Medicina Veterinaria. 2014;**28**:103-116

[46] Losa GA. The fractal geometry of life. Rivista di Biologia-Biology Forum. 2009;**102**(1):29-60

[47] Goto M, Oaki Y, Imai H. Dendritic growth of NaCl crystals in a gel matrix: Variation of branching and control of bending. Crystal Growth & Design. 2016;**16**(8):4278-4284

[48] Maragou M, Vaikousis E, Ntre A, Koronis N, Georgiou P, Hatzidimitriou E, et al. Tear and saliva ferning tests in Sjögren's syndrome (SS). Clinical Rheumatology. 1996;**15**(2):125-132

[49] Kogbe O, Liotet S, Tiffany JJM. Factors responsible for tear Ferning. Cornea. 1991;**10**(5):433-434

[50] Gómez Gómez JM, Medina J, Hochberg D, Mateo-Martí E, Martinez-Frias J, Rull F. Drying bacterial biosaline patterns capable of vital reanimation upon rehydration: Novel hibernating biomineralogical life formations. Astrobiology. 2014;**14**(7):589-602

[51] Desarnaud J, Derluyn H, Carmeliet J, Bonn D, Shahidzadeh N. Metastability limit for the nucleation of NaCl crystals in confinement. Journal of Physical Chemistry Letters. 2014;**5**(5):890-895

[52] Tabbara KF, Okumoto M. Ocular ferning test. A qualitative test for mucus deficiency. Ophthalmology. 1982;**89**(6):712-714

[53] Rolando M, Baldi F, Zingirian M. The effect of hyperosmolarity on tear mucus ferning. Fortschritte der Ophthalmologie. 1986;**83**(6):644-646

[54] Ravinder R, Kaipa O, Baddela VS, Singhal Sinha E, Singh P, Nayan V, et al. Saliva ferning, an unorthodox estrus detection method in water buffaloes (*Bubalus bubalis*). Theriogenology. 2016;**86**(5):1147-1155

[55] Menárguez M, Pastor LM, Odeblad E. Morphological characterization of different human cervical mucus types using light and scanning electron microscopy. Human Reproduction. 2003;**18**(9):1782-1789

[56] Gómez Gómez JM, Medina J, Rull F. A rich morphological diversity of biosaline drying patterns is generated by different bacterial species, different salts and concentrations: Astrobiological implications. Astrobiology. 2016;**16**(7):513-524

[57] Arakaki A, Shimizu K, Oda M, Sakamoto T, Nishimura T, Kato T. Biomineralization-inspired synthesis of functional organic/inorganic hybrid materials: Organic molecular control of self-organization of hybrids. Organic & Biomolecular Chemistry. 2015;**13**(4):974-989

[58] Li X, Chopp DL, Russin WA, Brannon PT, Parsek MR, Packman AI. Spatial patterns of carbonate biomineralization in biofilms. Applied and Environmental Microbiology. 2015;**81**(21):7403-7410

[59] Thorkelsson K, Bai P, Xu T. Self-assembly and applications of anisotropic nanomaterials: A review. Nano Today. 2015;**10**(1):48-66

[60] Hamley IW. Liquid crystal phase formation by biopolymers. Soft Matter. 2010;**6**(9):1863-1871

[61] Araki J, Kuga S. Effect of trace electrolyte on liquid crystal type of cellulose microcrystals. Langmuir. 2001;**17**(15):4493-4496

[62] Secor PR, Jennings LK, Michaels LA, Sweere JM, Singh PK, Parks WC, et al. Biofilm assembly becomes crystal clear—Filamentous bacteriophage organize the *Pseudomonas aeruginosa* biofilm matrix into a liquid crystal. Microbial Cell. 2016;**3**(1):49-52

[63] Unwin RR, Cabanas RA, Yanagishima T, Blower TR, Takahashi H, Salmond GPC, et al. DNA driven self-assembly of micron-sized rods using DNA-grafted bacteriophage fd virions. Physical Chemistry Chemical Physics. 2015;**17**(12):8194-8202

[64] Secor PR, Sweere JM, Michaels LA, Malkovskiy AV, Lazzareschi D, Katznelson E, et al. Filamentous bacteriophage promote biofilm assembly and function. Cell Host & Microbe. 2015;**18**(5):549-559

[65] Tomar S, Green MM, Day LA. DNA-protein interactions as the source of large-length-scale chirality evident in the liquid crystal behavior of filamentous bacteriophages. Journal of the American Chemical Society. 2007;**129**(11):3367-3375

[66] Secor PR, Michaels LA, Smigiel KS, Rohani MG, Jennings LK, Hisert KB, et al. Filamentous bacteriophage produced by *Pseudomonas aeruginosa* alters the inflammatory response and promotes noninvasive infection in vivo. Infection and Immunity. 2017;**85**(1):1-11

[67] Penner JC, Ferreira JAG, Secor PR, Sweere JM, Birukova MK, Joubert L, et al. Pf4 bacteriophage produced by *Pseudomonas aeruginosa* inhibits Aspergillus fumigatus metabolism via iron sequestration. Microbiology. 2016;**162**(9):1583-1594

[68] Vallooran JJ, Handschin S, Pillai SM, Vetter BN, Rusch S, Beck HP, et al. Lipidic cubic phases as a versatile

platform for the rapid detection of biomarkers, viruses, bacteria, and parasites. Advanced Functional Materials. 2016;**26**(2):181-190

[69] Stewart PS, Franklin MJ. Physiological heterogeneity in biofilms. Nature Reviews Microbiology. 2008;**6**(3):199-210

[70] Freitas F, Alves VD, Pais J, Costa N, Oliveira C, Mafra L, et al. Characterization of an extracellular polysaccharide produced by a pseudomonas strain grown on glycerol. Bioresource Technology. 2009;**100**(2):859-865

[71] Kim JS, Kuk E, Yu KN, Kim J-H, Park SJ, Lee HJ, et al. Antimicrobial effects of silver nanoparticles. Nanomedicine. 2007;**3**(1):95-101

[72] Mezger TG. The Rheology Handbook. 4th ed. Vincentz Network GmbH & Co KG. Hanover; 2014. 434 p